

Calorimetric study of the nematic to smectic-A phase transition in octylcyanobiphenyl-hexane binary mixtures

Krishna P. Sigdel and Germano S. Iannacchione*

*Department of Physics, Worcester Polytechnic Institute,
Worcester, Massachusetts 01609, USA*

(Dated: February 5, 2022)

Abstract

The continuous nematic to smectic-A (N -SmA) phase transition has been studied by high-resolution ac-calorimetry in binary mixtures of the liquid crystal octylcyanobiphenyl(8CB) and a non-mesogenic, low-molecular weight, solvent n-hexane(hex) as a function of temperature and solvent concentration. Heating and cooling scans about the N -SmA transition temperature were repeatedly performed on pure and six 8CB+hex samples having hexane molar concentration ranging from $x_{hex} = 0.02$ to 0.12 . All 8CB+hex samples in this range of x_{hex} remain macroscopically miscible and exhibit an N -SmA heat capacity peak that shifts non-monotonically to lower temperature and evolves in shape, with a reproducible hysteresis, as x_{hex} increases. The imaginary part of heat capacity remains zero up to $x_{hex}^{TCP} \simeq 0.07$ above which the distinct peak is observed, corresponding to a jump in both the real and imaginary enthalpy. A simple power-law analysis reveals an effective exponent that increases smoothly from 0.30 to 0.50 with an amplitude ratio $A^-/A^+ \rightarrow 1$ as $x_{hex} \rightarrow x_{hex}^{TCP}$. This observed crossover towards the N -SmA tricritical point driven by solvent concentration is consistent with previous results and can be understood as weakening of the liquid crystal intermolecular potential promoting increased nematic fluctuations.

PACS numbers: 61.30.-v, 64.70.mj, 65.40.Ba

* electronic address: gsiannac@wpi.edu

I. INTRODUCTION

Liquid crystals(LCs) are anisotropic fluids which exhibit a varieties of phases and phase transitions [1, 2]. The nematic and smectic-*A* phases are the best known phases of liquid crystals. The transition between nematic (*N*) and smectic-*A* (Sm*A*) phases is interesting and important because it involves the breaking of a continuous symmetry as well as sharing some properties with the superconducting transition in metals and the superfluid transition in ^4He . The *N*-Sm*A* transition is also a model phase transition for the study of confinement and disorder effects such as in mixtures with silica aerosil [3–5], or embedded in an aerogel [6, 7] and controlled porous glass [8–10]. The phase transition behavior is also sensitive to an applied external electric and magnetic field [11, 12] as well as with LC+LC mixtures [13–17]. Even though the *N*-Sm*A* transition has been extensively studied [18], there remains many unresolved issues regarding the fundamental nature of the transition.

Recently, attention has been drawn to the study of miscible mixtures of liquid crystals and non-mesogenic, low-molecular weight, solvents for broadening the basic understanding of mesogenic order, critical behavior and tuning viscoelastic properties [19–23]. X-ray diffraction experiments performed on smectic-*A* and smectic-*C* thermotropic liquid crystals have demonstrated that the smectic layer spacing increases with the addition of organic solvents to the host liquid crystal indicating the formation of an organic lyotropic lamellar liquid crystal phase[23]. It was suggested from the visual inspection that for octylcyanobiphenyl (8CB) and n-hexane(hex) mixture systems (having a volume fraction of ≥ 0.1), the solvent is not uniformly distributed throughout the host LC and minimal, non-reproducible, swelling occurs. It was also suggested that the amount of solvent incorporated in a smectic liquid crystal depends on the host liquid crystal, nature and amount of solvent, and temperature; noting that the mixture phase separates for a solvent to liquid crystal mole ratio ≥ 1.0 . Other studies of the effect of a biphenyl solvent on the splay and bend elastic constant and the rotational viscosity coefficient of 8CB observed an anomalous behavior of K_{11} and $\Delta\epsilon$ near *N*-Sm*A* transition[24]. A theoretical study on the influence of non-mesogenic solvent on the *N*-Sm*A* phase transition using Landau approach found a concentration induced tricritical point for the *N*-Sm*A* transition[21]. This theoretical model also found that the Frank elastic constants K_{11} , K_{22} , and K_{33} are modified as a function of solvent concentration near the *N*-Sm*A* phase transition.

A recent calorimetric study of the N -SmA transition in mixtures of 8CB and cyclo-hexane (8CB+chex) was performed under continuous stirring conditions [19]. This study found a linear decrease of the transition temperatures T_{NA} with a linear increase of critical heat capacity exponent α with increasing mole fraction of cyclohexane x_{chex} . This behavior ends at a tricritical point (TCP) where the transition becomes first-order at $x_{chex}^{TCP} = 0.046$, just below which $\alpha = 0.5$ and the nematic range $\Delta T_N = T_{IN} - T_{NA} = 4.8K$. For $x_{chex} > x_{chex}^{TCP}$, the N -SmA latent heat smoothly increases non-linearly from zero [19].

The N -SmA phase transition is a non-trivial member of the 3D-XY universality class due to the anisotropy of its critical fluctuations parallel and perpendicular to the director [18, 25, 26]. The N -SmA critical behavior is strongly effected by the coupling between the smectic order parameter $\psi(\vec{r}) = \psi_0 \exp(i\vec{q}_0 \cdot \vec{r})$ and the nematic order parameter $Q_{ij} = (1/2)S(3\hat{n}_i\hat{n}_j - \delta_{ij})$. Here, the ψ is the amplitude of the one-dimensional density wave, $\rho(\vec{r}) = Re[\rho_0 + \exp(i\vec{q}_0 \cdot \vec{r})\psi(\vec{r})]$, $q_0 = 2\pi/d$ is the wave vector corresponding to the layer spacing d , S is a scalar parameter measuring the magnitude of orientational order on short length scales, and \hat{n} is the nematic director describing spatial orientation of the orientational axis on longer length scales. It has been shown by de Gennes [1] and McMillan [27] that a mean-field coupling between S fluctuations and smectic order $\delta S - \psi$ can drive a second-order N -SmA phase transition first-order via a tricritical point. The theory proposed by Halperin, Lubenski, and Ma (HLM) [28, 29], taking into account the coupling between ψ and the nematic director fluctuations $\delta\hat{n}$, showed that the N -SmA transition is always at least weakly first order which rules out the possibility of a tricritical point. Combining both the δS and $\delta\hat{n}$ couplings introduces two more terms in free energy expression as compared to the usual standard form. One term is of the form $\psi^2 S$ which is nematic-smectic order parameter coupling (referred to as de Gennes coupling) and the other is smectic order-nematic director fluctuation coupling (HLM coupling) $\psi^2 \delta\hat{n}$. The former coupling reveals the effects of the elasticity of the nematic order prior to the onset of the smectic order and can drive the N -SmA transition from XY like to tricritical to weakly first-order[3]. The coupling $\psi^2 \delta\hat{n}$ causes the anisotropic elastic deformations in the smectic. The strength of this coupling depends on the magnitude of the splay elastic constant K_{11} which is directly proportional to S^2 . Since it is expected that a low-molecular weight solvent miscible in an LC would affect both δS and $\delta\hat{n}$ fluctuations, the x_{sol} dependence would be accounted for using similar terms in a free-energy expansion.

In this work, the effect of a non-mesogenic, low molecular weight, solvent (n-hexane) concentration on the continuous nematic to smectic-*A* (*N-SmA*) phase transition on octylcyanobiphenyl (8CB) and n-hexane (hex) binary mixtures (8CB+hex) was studied via high-resolution ac-calorimetry as a function of n-hexane concentration, x_{hex} . The introduction of n-hexane on 8CB causes a dramatic change in the *N-SmA* phase transition behavior. The heat capacity peaks associated with the *N-SmA* transition, δC_p , shift towards lower temperature non-monotonically and become progressively larger as the hexane concentration increases. The dispersive part of heat capacity C_p'' associated with *N-SmA* transition has peaks only for higher hexane mole fractions ($x_{hex} \geq 0.08$) but not for the lower hexane mole fractions ($x_{hex} \leq 0.06$) revealing the continuous (second order) nature of the *N-SmA* transition for the lower n-hexane mole fractions ($x_{hex} \leq 0.06$) and first-order nature for higher n-hexane mole fractions ($x_{hex} \geq 0.08$). The integrated ac-enthalpy increases overall as a function of hexane molar fraction whereas the imaginary part of the enthalpy reveals a sharp increase at hexane mole fraction of around 0.07 and remains fairly constant. The crossover between continuous to first-order *N-SmA* transition is observed at a tricritical point of $x_{hex}^{TCP} \approx 0.07$. The non-linear increase in the heat capacity effective critical exponent towards its tricritical value ($\alpha = 0.5$) is observed.

The hysteresis of the δC_p shape on heating and cooling has been observed is likely due to a microscopic phase separation of the solvent, perhaps into interstitial region between smectic layers. The non-monotonic transition temperature shift may be due to the competing interactions of microphase separation and dilution effects. These effects may also responsible for the α_{eff} behavior with extended curvature as $x_{hex} \rightarrow x_{hex}^{TCP}$. These effects would also have profound consequences on the higher temperature *I-N* phase transition as well, which was presented in previous paper [30].

This paper is organized as follows; following this introduction, Section II describes the preparation of sample, the calorimetric cell, and the ac-calorimetric procedures employed in this work. Section III describes the calorimetric results and critical behavior of the *N-SmA* phase transition in the 8CB+hex system. Section IV discusses these results and draws conclusions.

II. EXPERIMENTAL

The liquid crystal 8CB has a molecular mass $M_w = 291.44 \text{ g mol}^{-1}$ and a density of $\rho_{LC} = 0.996 \text{ g ml}^{-1}$. The 8CB, purchased from Frinton Lab, was degassed under vacuum for about two hours in the isotropic phase before used for pure and mixture samples. Spectroscopic grade n-hexane (molecular mass of 86.18 g mol^{-1} , a density of 0.6548 g ml^{-1} , and a boiling point of 342 K) purchased from EM Science was used without further purification. The 8CB and n-hexane mixtures appear to be miscible up to an n-hexane mole fraction of ≥ 0.12 . This was confirmed by polarizing micrographs of the samples. Measurements were performed on samples as a function of n-hexane mole fraction x_{hex} ranging from 0 (pure 8CB) to 0.12.

High resolution ac-calorimetric measurements were carried out using a homemade calorimeter. The calorimetric sample cell consists of an aluminium envelop $15 \times 8 \times 0.5 \text{ mm}$. To prepare an envelop cell, a sheet of aluminum was cleaned using successive application of water, ethanol, and acetone in an ultrasonic bath and then was folded and sealed on three sides with super-glue (cyanoacrylate). Once the cell was thoroughly dried, the desired amount of liquid crystal followed by a relatively large amount of n-hexane were introduced to the cell. The mass of the sample and cell was monitored as the n-hexane was allowed to evaporate slowly until the desired mass of the n-hexane was achieved. At the point of the desired mass of the 8CB+hex mixture, the envelop flap was quickly folded and sealed with the super-glue. When the filled cell was ready a 120Ω strain gauge and $1 \text{ M}\Omega$ carbon-flake thermistor were attached to opposite surfaces of the cell using GE varnish. The cell was then mounted into the calorimeter, the details of which can be found elsewhere [31–33]. In the ac-mode, oscillating heating power $P_{ac}e^{i\omega t}$ is input to the cell resulting in temperature oscillations with an amplitude T_{ac} and a relative phase shift, $\varphi = \Phi + \pi/2$, where Φ is the absolute phase shift between T_{ac} and the input power. Defining the heat capacity amplitude as $C^* = P_{ac}/(\omega T_{ac})$, the specific heat at a heating frequency ω can be expressed as

$$C_p = \frac{C'_{filled} - C_{empty}}{m_s} = \frac{C^* \cos(\varphi) - C_{empty}}{m_s} \quad (1)$$

$$C_p'' = \frac{C''_{filled}}{m_s} = \frac{C^* \sin(\varphi) - \frac{1}{\omega R_e}}{m_s} \quad (2)$$

where C'_{filled} and C''_{filled} are the real and imaginary parts of the heat capacity, C_{empty} is the heat capacity of the empty cell, m_s is the mass of the sample (in the range of 15 mg to 40 mg),

and R_e is the external thermal resistance between the cell and the bath. Eq. (1) and (2) need small correction to account the non-negligible internal thermal resistance as compared to R_e and this was applied to all samples [34]. The real part of the heat capacity indicates storage (capacitance) of the energy whereas the imaginary part indicates the loss (dispersion) of energy in the sample. Temperatures corresponding to equilibrium, one-phase states exhibit a flat imaginary part of heat capacity, i.e. $C_p'' = 0$ [35]. Non-equilibrium dispersive regions, such as a two-phase coexistence region where the latent heat is released, have non-zero C_p'' .

Figure 1 illustrates the specific heat capacity variation over an extended temperature range for the $x_{hex} = 0.02$ 8CB+hex sample. The dashed curve under the N -SmA heat capacity peak represents the I - N specific heat capacity wing C_p^{wing} expected in the absence of the N -SmA transition. This wing is used to determine the excess specific heat associated with the N -SmA phase transition

$$\delta C_p = C_p - C_p^{wing}. \quad (3)$$

The enthalpy change associated with a phase transition is defined as

$$\delta H = \int \delta C_p dT. \quad (4)$$

For a second-order or continuous phase transition, the limits of integration are as wide as possible about the δC_p peak and gives the total enthalpy change (δH) associated with the transition. But for a first-order transition the situation is complicated due to the presence of a coexistence region as well as a latent heat ΔH . The total enthalpy change for a weakly first order phase transitions is the sum of the integrated enthalpy and the latent heat, $\Delta H_{total} = \delta H + \Delta H$. Due to partial phase conversion during a T_{ac} cycle, typical δC_p values obtained in the two-phase coexistence region are artificially high and frequency dependent. A simple integration of the observed δC_p peak yields an effective enthalpy change δH^* for the first-order transition which includes some of the latent heat contribution. If we integrate the imaginary part of heat capacity given by Eq. (2), we can get the imaginary transition enthalpy $\delta H''$, which is the dispersion of energy in the sample and is a proxy of latent heat associated with the transition. In an ac-calorimetric technique the uncertainty in determining the enthalpy is typically 10% due to the uncertainty in the baseline and background subtraction.

III. RESULTS

A. The N -SmA Heat Capacity

The resulting δC_p data of the N -SmA transition on heating for 8CB+hex and pure 8CB samples over a $\pm 1.5K$ temperature range window about the δC_p peak is shown in Fig. 2 (upper panel). As the mole fraction of n-hexane increases, the N -SmA heat capacity peak becomes larger than the pure N -SmA peak and with apparently larger wings on the high temperature side of the peak. Figure 2 (lower panel) shows the imaginary part of specific heat C_p'' on heating as a function of temperature about T_{NA} . For the n-hexane mole fractions $x_{hex} \leq 0.06$, the C_p'' is flat, indicating the second-order nature of the transition. For $x_{hex} \geq 0.08$, the C_p'' reveals a peak indicating a first-order behavior of the transition. As the mole fraction of n-hexane increases beyond $x_{hex} \geq 0.08$, the C_p'' peak become broader with a two-phase co-existence region growing from $\sim 0.35K$ at $x_{hex} = 0.08$ to $\sim 0.85K$ at $x_{hex} = 0.12$.

The N -SmA excess specific heat δC_p (upper panel) and imaginary part of heat capacity C_p'' (lower panel) on cooling are shown in Fig. 3. On cooling, the δC_p peaks exhibit larger C_p wings on both sides of T_{NA} but the low temperature wing appears progressively smeared in temperature. In addition, the δC_p on cooling exhibits sharp peaks up to $x_{hex} = 0.08$ then appears rounded for $x > 0.08$. The N -SmA C_p'' behavior on cooling is similar to the heating scans in that $C_p'' = 0$ through T_{NA} for $x_{hex} \leq 0.06$, then reveals a peak for $x_{hex} \geq 0.08$. This indicates, as on heating, a cross-over from continuous to first-order transition behavior. However, the C_p'' peaks for $x_{hex} \geq 0.08$ on cooling have markedly different shape than on heating. Here, as the temperature approaches T_{NA} from above, a sharp jump preceded by a relatively small wings occurs at $\sim 0.1K$ above T_{NA} for all 8CB+hex samples. As the temperature cools further, a long C_p'' tail is seen to a common trend at $\sim -0.25K$ for $x_{hex} = 0.08$ and $\sim -0.4K$ for $x_{hex} = 0.09$ and 0.12 below T_{NA} . The increase in the two-phase co-existence is similar to that seen on heating.

The N -SmA transition temperature T_{NA} is defined as the temperature of the δC_p peak maximum and the I - N transition temperature is taking at the lowest temperature of the isotropic phase prior to entering the $I+N$ two-phase coexistence region[30]. Figure 4 (upper panel) shows the I - N and N -SmA phase transition temperatures as a function of x_{hex} . As

x_{hex} increases, both transition temperatures decrease non-linearly with a bump at $x_{hex} \sim 0.07$. Figure 4(lower panel) shows the nematic temperature range $\Delta T_N = T_{IN} - T_{NA}$ as a function of x_{hex} revealing a similar non-linear trend with a similar bump at the same x_{hex} . The horizontal dashed, dashed dot, and dot lines represent nematic ranges for pure 9CB[36], 8CB+chex[19], and 8CB+10CB [15] at the tricritical point respectively. The solid straight lines are the transition temperatures (Fig. 4-upper panel) and nematic range (Fig. 4-lower panel) for the 8CB+chex system [19]

Since continuous transition behavior is observed for $x_{hex} = 0.06$ and first-order behavior at $x_{hex} = 0.08$, a tricritical point mole fraction is taken as $x_{hex}^{TCP} = 0.07$ with the corresponding nematic range at $\Delta T_N^{TCP} \simeq 4.63K$. The vertical dashed line in both the panels of Fig. 4 indicates x_{hex}^{TCP} and a bold-bordered box in the lower-panel gives the location of the cross-over point whose width and height are the magnitude of uncertainties in x_{hex}^{TCP} and ΔT_N^{TCP} respectively.

The effective N -SmA transition enthalpy δH_{NA}^* was obtained by integrating δC_p in the range $\pm 3K$ about T_{NA} . The dispersive enthalpy, $\delta H_{NA}''$ of the N -SmA transition, available only for $x_{hex} \geq 0.08$, and was obtained by integrating the N -SmA C_p'' peak. Since a fixed heating frequency was used, the non-zero $\delta H_{NA}''$ is only proportional to the transition latent heat. The resulting δH_{NA}^* and $\delta H_{NA}''$ for heating (\circ) and cooling (\bullet) scans as a function of x_{hex} for all 8CB+hex samples are shown in Fig. 5. The δH_{NA}^* values show an overall increase in value with increasing x_{hex} and are consistent on heating and cooling. A small apparent jump in δH_{NA}^* is seen at $\sim x_{hex}^{TCP}$. See Figure 5(upper panel). The $\delta H_{NA}''$ exhibits a sudden jump from 0 to $\sim 0.28 J/g$ at x_{hex}^{TCP} .

A summary of these results for 8CB+hex samples including pure 8CB is tabulated in Table I. Included are the n-hexane molar fraction x_{hex} , the N -SmA transition temperatures T_{NA} , nematic range ΔT_N , integrated enthalpy change δH_{NA}^* , imaginary enthalpy $\delta H_{NA}''$, McMillan ratio MR and height of excess heat capacity peaks h_M for all the 8CB+hex samples including pure 8CB.

B. Power-law Analysis of N -SmA phase transition

Because the δC_p for the N -SmA transition in 8CB+hex remains continuous and sharp for $x_{hex} \leq x_{hex}^{TCP}$, a critical power-law analysis was performed. The usual power law form in

terms of reduced temperature, $|t| = |(T - T_c)|/T_c$, that is used to analyze the excess specific heat associated with N -SmA transition is given by[18]

$$\delta C_p = A^\pm |t|^{-\alpha} (1 + D_1^\pm |t|^{\Delta_1}) + B_c, \quad (5)$$

where B_c is the critical background, A^\pm are the amplitudes above and below the transition, D_1^\pm are the correction-to-scaling amplitude with an exponent $\Delta_1 = 0.524$ [18]. A full, non-linear, fitting of Eq.(5) to the δC_p data was attempted, but because the number of data close to the peak were relatively sparse, these fits did not properly converge.

A simple power-law analysis procedure was employed in order to estimate the variation of the critical exponent α as a function of x_{hex} . This procedure begins by approximating T_c for each continuous δC_p peak. This is done by plotting a $\log(\delta C_p)$ vs $\log(|t|)$ and choosing T_c such that the high and low temperature wings appear linear and parallel to each other for low $|t|$. The rounded and non-power-law data points are easily determined and removed.

Figure 6 shows the resulting log-log plot of data above and below T_c for pure 8CB ($x_{hex} = 0$) and the highest concentration 8CB+hex sample that is continuous as determined by C_p'' ($x_{hex} = 0.06$). Now, a range of data up to $|t_{max}|$ was chosen in order to perform a simple linear fit, $\log(\delta C_p) = \log(A^\pm) - \alpha'_{eff} \log|t|$. Here, $|t_{max}|$ varied smoothly from 8.9×10^{-4} for pure 8CB to 1.8×10^{-3} for the $x_{hex} = 0.06$ 8CB+hex sample. The resulting linear fits are shown in Fig. 6 for data above and below T_c . The difference between $\alpha'_{eff}(T > T_c)$ and $\alpha'_{eff}(T < T_c)$ is taken as the uncertainty in α'_{eff} . The resulting α'_{eff} are not the true critical exponents because of this simplified analysis. However, comparing the pure 8CB result here to the literature value of $\alpha_{eff} = 0.3$ [3], a corrected α_{eff} for the 8CB+hex samples is taken as an algebraic shift of +0.17, which is the difference of $\alpha'_{eff} - \alpha_{eff}$ for pure 8CB. This procedure was applied for all samples from $x_{hex} = 0$ to 0.06 and should reasonably approximate the x_{hex} dependence of α_{eff} .

The resulting estimate of the N -SmA heat capacity effective critical exponent as a function of x_{hex} are shown in Fig. 7. Here, a linear rapid rise in α_{eff} is seen as x_{hex} increases from 0 to 0.04 then curving over for $x_{hex} > 0.04$. The upward arrow in Fig. 7 is the best estimate of x_{hex}^{TCP} for this 8CB+hex system.

IV. DISCUSSION AND CONCLUSION

The continuous N -SmA liquid crystal phase transition has been studied using high-resolution ac-calorimetry as a function of solvent dopant concentration. Multiple heating and cooling cycles reproduce each other for $x_{hex} \leq 0.12$ along with no visual indication of phase separation support the view that the 8CB+hex binary system remained mixed (n-hexane miscible) for all samples studied here, without mechanical mixing. This is supported also by x-ray studies of the smectic layer spacing in 8CB+hex that showed phase separation for $x_{hex} > 1.0$ [23]. In this work, the smectic layer spacing increased with increasing x_{hex} and was interpreted as a nano-scale partitioning of n-hexane in between smectic layers.

A more recent calorimetric study of binary mixtures of 8CB with various, low-molecular weight, solvents found dramatic changes to the character of the N -SmA phase transition [19]. In this work, the N -SmA transition approaches a tricritical point linearly. However, this study used cyclo-hexane, that has ring structure and employed continuous mixing during measurements as a function of cyclohexane mole-fraction, x_{chex} . The transition temperature T_{NA} decreases linearly as x_{chex} increases, the critical exponent α increases linearly from 0.31 (pure 8CB) to 0.50 at $x_{chex} = 0.046$, and the onset of a N -SmA latent heat occurs smoothly at TCP, $x_{chex}^{TCP} = 0.046$. These results were modelled using mean-field Landau-deGennes theory incorporating the nematic free-energy, smectic free-energy, and a coupling between nematic and smectic order parameters. This model was extended to account for the solvent by adding a solvent mole-fraction coupling to ψ^2 and to $\psi^2 \delta S$ to the total solvent free-energy.

Similar results were found in 8CB+biphenyl binary mixtures and a Landau-de Gennes model that accounted for change in the LC elastic constants with x_{sol} . However, TCP was not found in 8CB+biphenyl system [24].

In this present study, several important differences emerge. As x_{hex} increases, T_{NA} decreases as well as the nematic range ΔT_N in a non-linear way. The character of N -SmA transition remains continuous up to $x_{hex} \simeq 0.07$ where it appears to jump suddenly to a first-order transition. The bump in T_{NA} and ΔT_N as well as the jump in $\delta H_{NA}''$ all occur at x_{hex}^{TCP} .

The critical behavior, estimated by the simple power-law analysis presented here, evolves with α_{eff} initially increases linearly as in the 8CB+chex system but then curves over to reach $\alpha_{eff} = 0.50$ at $x_{hex} \rightarrow x_{hex}^{TCP}$. Qualitatively, the correction-to-scaling terms D^\pm and

the amplitude ratio A^-/A^+ are changing their values towards the tricritical values as a function of x_{hex} . Here, the qualitative measurement of the amplitude ratio A^-/A^+ was extracted examining the gap between two slope lines of the linear fit of log-log plot of δC_p vs $|t|$ (Fig. 6) and the curvature of the curve at high $|t|$ was observed to get qualitative measure of D^\pm .

The addition of n-hexane in 8CB creates the random dilution effect which causes the decrease in transition temperature T_{NA} and nematic range ΔT_{NA} . The experiment was done without stirring the sample which may cause some phase separation in microscopic or even in nanoscopic scale. These dilution and microphase separation effects, may cause to develop the two competing interactions which cause the non-linearity in the transition temperature T_{NA} , nematic range ΔT_N , effective critical exponent α_{eff} and jump in the imaginary enthalpy $\delta H_{NA}''$. These effects also cause the change in coupling between the order parameters ψ and Q which consequently change the order of the N -SmA phase transition from continuous to first order with a critical point at $x_{hex}^{TCP} \simeq 0.07$.

We have undertaken a detailed calorimetric studies on the effect of non- mesogenic, low molecular weight solvent(hexane) on octylcyanobiphenyl(8CB) phase transitions with emphasis on the most extensively studied but controversial N -SmA phase transition. The addition of the hexane on 8CB dilutes the mixture and changes the intermolecular potential. The microscopic phase separation and dilution effect due to the introduction of n-hexane in 8CB cause the change in magnitude of S - ψ and $\psi - \delta\hat{n}$ couplings which consequently change the phase transition behavior. The result obtained reveals new aspect of the effect of non-mesogenic disorder on the liquid crystal transition.

Acknowledgments

This work was supported by the Department of Physics at WPI.

-
- [1] P. G. de Gennes and J. Prost, *The Physics of Liquid Crystals* (Oxford University Press, Clarendon, Oxford, England, 1993).
 - [2] S. Chandrashekhara, *Liquid Crystals* (Cambridge University Press, England, 1992).
 - [3] G. S. Iannacchione, S. Park, C. W. Garland, R. J. Birgeneau, and R. L. Leheny, Phys. Rev. E **67**, 011709 (2003).
 - [4] G. S. Iannacchione, Fluid Phase Equilibria **222/223**, 177 (2004).
 - [5] F. Cruceanu, D. Liang, R. L. Leheny, C. W. Garland, and G. S. Iannacchione, Phys. Rev. E **79**, 011710 (2009).
 - [6] L. Wu, B. Zhou, C. W. Garland, T. Bellini, and D. W. Schaefer, Phys. Rev. E **51**, 2157 (1995).
 - [7] T. Bellini, L. Radzihosky, J. Toner, and N. A. Clark, Science **294**, 1074 (2001).
 - [8] A. Zidansek, G. Lahajnar, and S. Kralj, Appl. Magn. Reson. **27**, 311 (2004).
 - [9] Z. Kutnjak, S. Kralj, G. Lahajnar, and S. Zumer, Phys. Rev. E **68**, 021705 (2003).
 - [10] Z. Kutnjak, S. Kralj, G. Lahajnar, and S. Zumer, Fluid Phase Equilibria **222-223**, 275 (2004).
 - [11] R. Mukhopadhyay, A. Yethiraj, and J. Bechhoefer, Phys. Rev. Lett. **83**, 4796 (1999).
 - [12] A. Primak, M. Fisch, and S. Kumar, Phys. Rev. Lett. **88**, 035701 (2002).
 - [13] K. J. Stine and C. W. Garland, Phys. Rev. A **39**, 3148 (1989).
 - [14] M. B. Sied, J. Salud, D. O. Lopez, M. Barrio, and J. L. Tamarit, Phys. Chem. Chem. Phys. **4**, 2587 (2002).
 - [15] M. G. Lafouresse, M. B. Sied, H. Allouchi, D. O. Lopez, J. Salud, and J. L. Tamarit, Chem. Phys. Lett. **376**, 188 (2003).
 - [16] M. B. Sied, D. O. Lopez, J. L. Tamarit, and M. Barrio, Liquid Crystals **29**, 57 (2002).
 - [17] S. Jeong, D. Kim, K. Rhie, M. Hong, S. Kumar, W. Jang, , and S. Shin, Journal of Physics D: Applied Physics **41**, 062002 (2008).
 - [18] C. W. Garland and G. Nounesis, Phys. Rev. E **49**, 2964 (1994).
 - [19] K. Denolf, G. Cordoyiannis, C. Glorionx, and J. Thoen, Phys. Rev. E **76**, 051702 (2007).
 - [20] K. Denolf, B. V. Roie, C. Glorionx, and J. Thoen, Phys. Rev. Lett. **97**, 107801 (2006).
 - [21] P. K. Mukherjee, J. Chem. Phys. **116**, 9531 (2002).
 - [22] S. DasGupta and S. K. Roy, Phys. Lett. A **288**, 323 (2001).
 - [23] T. P. Rieker, Liquid Crystals **19**, 497 (1995).

- [24] S. DasGupta and P. C. ans Soumen Kumar Roy, Phys. Rev. E **63**, 041703 (2001).
- [25] A. Yethiraj, R. Mukhopadhyay, and J. Bechhoefer, Phys. Rev. E **65**, 021702 (2002).
- [26] C. W. Garland and G. S. Iannacchione, J. Phys. Chem. B **113**, 3901 (2008).
- [27] W. L. McMillan, Phys. Rev. A **4**, 1238 (1971).
- [28] B. Halperin, T. C. Lubensky, and S. K. Ma, Phys. Rev. Lett. **32**, 292 (1974).
- [29] M. Anisimov, P. Cladis, E. E. Gorodetskii, D. A. Huse, V. E. Podneks, V. Taratuta, W. van Saarloos, and V. P. Voronov, Phys. Rev. A **41**, 6749 (1990).
- [30] K. P. Sigdel and G. S. Iannacchione, Submitted to J. chem. Phys. (2010).
- [31] P. F. Sullivan and G. Seidel, Phys. Rev. **173**, 679 (1968).
- [32] D. Finotello, S. Qian, and G. S. Iannacchione, Thermochemica Acta **304/305**, 303 (1997).
- [33] H. Yao and C. W. Garland, Rev. Sci. Instrum. **69**, 172 (1998).
- [34] A. Roshi, G. S. Iannacchione, P. S. Clegg, and R. J. Birgeneau, Phys. Rev. E **69**, 031703 (2004).
- [35] G. S. Iannacchione, C. W. Garland, J. T. Mang, and T. P. Rieker, Phys. Rev. E **58**, 5966 (1998).
- [36] S. Qian, G. S. Iannacchione, and D. Finotello, Phys. Rev. E **57**, 4305 (1998).

Figures

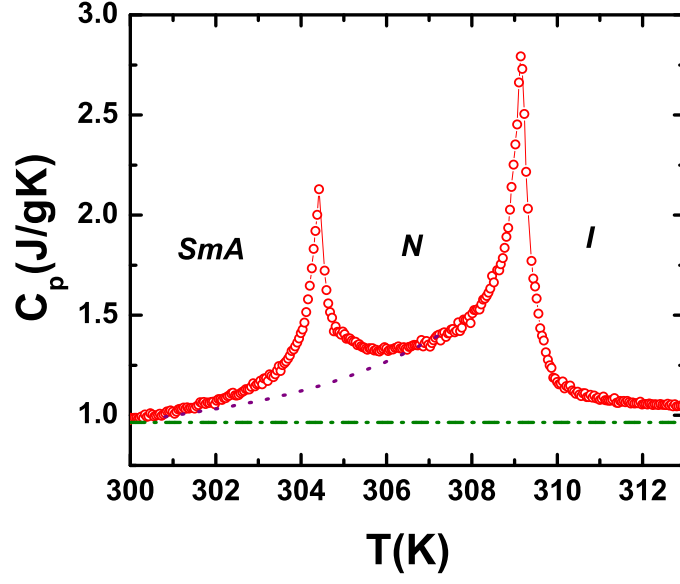


FIG. 1: Specific heat capacity for an 8CB+hex sample on heating with $x_{hex} = 0.02$. The dashed dotted line represents the C_p background, while the dashed curve acts as C_p^{wing} and represents the low temperature *I-N* C_p wing that would be expected in the absence of *N-SmA* transition.

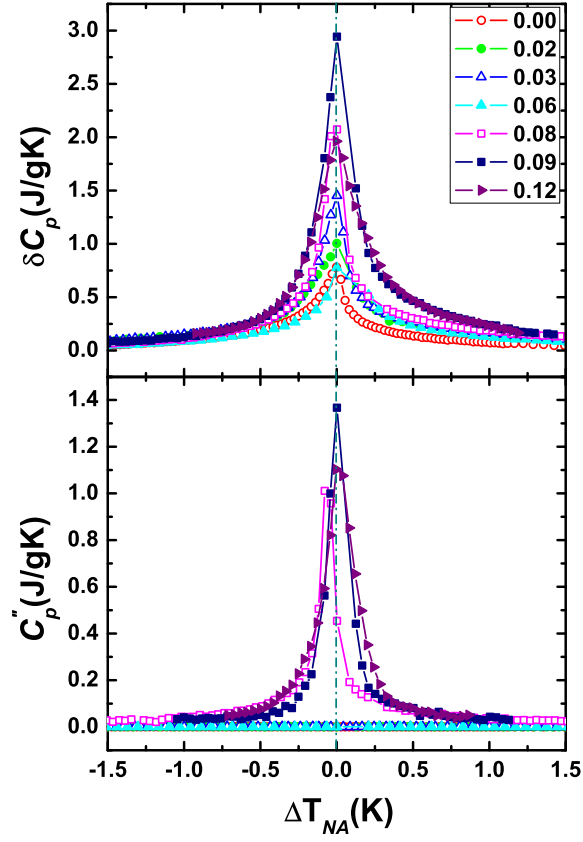


FIG. 2: Upper panel: The excess specific heat δC_p associated with the N -SmA transition on heating as a function of temperature about T_{NA} for pure and all 8CB+hex samples. See legend. Lower panel: The imaginary part of heat capacity on heating for all samples as a function of temperature about T_{NA} .

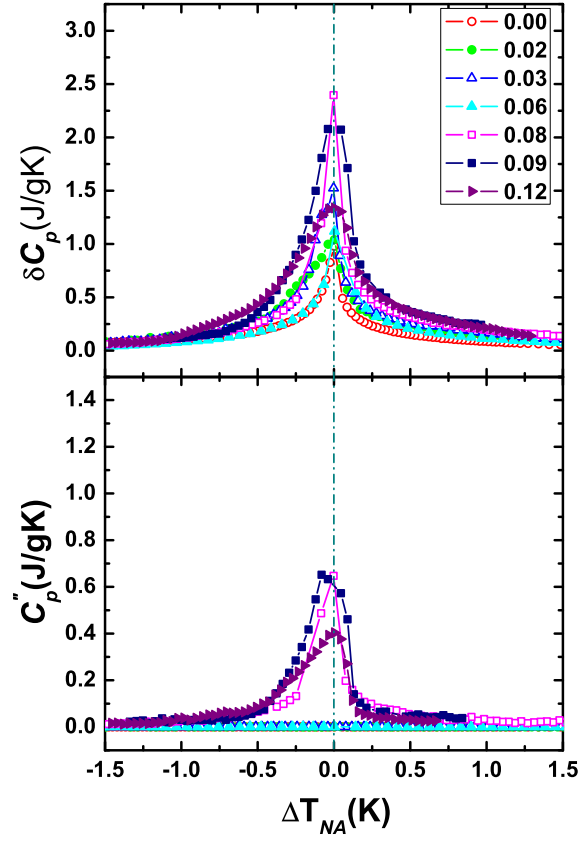


FIG. 3: Upper panel: The excess specific heat δC_p associated with the N -SmA transition on cooling as a function of temperature about T_{NA} for pure and all 8CB+hex samples. The definition of the symbols are given on the inset. Lower panel: The imaginary part of heat capacity on cooling for all samples as a function of temperature about T_{NA} .

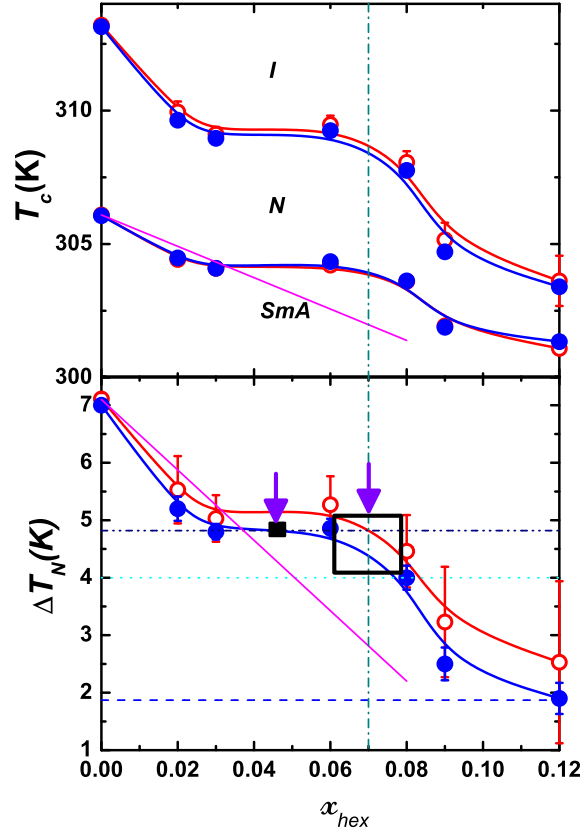


FIG. 4: Upper Panel: The I - N and N - SmA phase transition temperatures on heating (\circ) and cooling (\bullet) as a function of x_{hex} . Solid lines are guides to the eye. Lower panel: The nematic temperature range ΔT_N on heating (\circ) and cooling (\bullet) as a function of x_{hex} . The closed and open rectangular boxes represent the position of tricritical points for 8CB+chex [19] and 8CB+hex systems respectively and the width and height of the boxes represent the uncertainties on x_{hex}^{TCP} and ΔT_N^{TCP} respectively. The horizontal dashed, dashed dot, and dot lines are nematic ranges for pure 9CB[36], 8CB+chex, and 8CB+10CB [15] respectively at tricritical point. The solid straight lines are transition temperature (upper panel) and nematic range (lower panel) for 8CB+chex system [19].

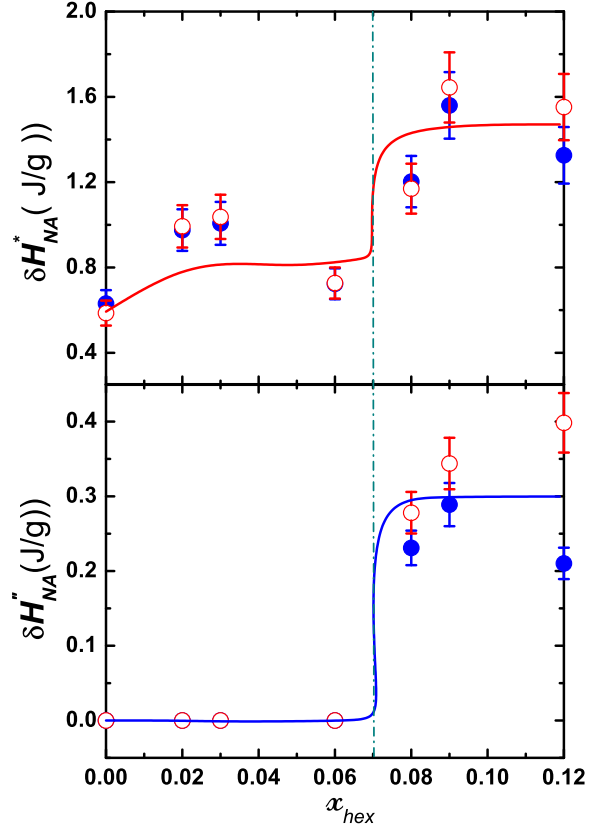


FIG. 5: Upper panel: The total integrated δC_p ac-enthalpy δH_{NA}^* on heating (\circ) and cooling (\bullet) as the function of x_{hex} . Lower panel: Integrated C_p'' enthalpy $\delta H_{NA}''$ on heating (\circ) and cooling (\bullet) as the function of x_{hex} . Solid lines are guides to the eye.

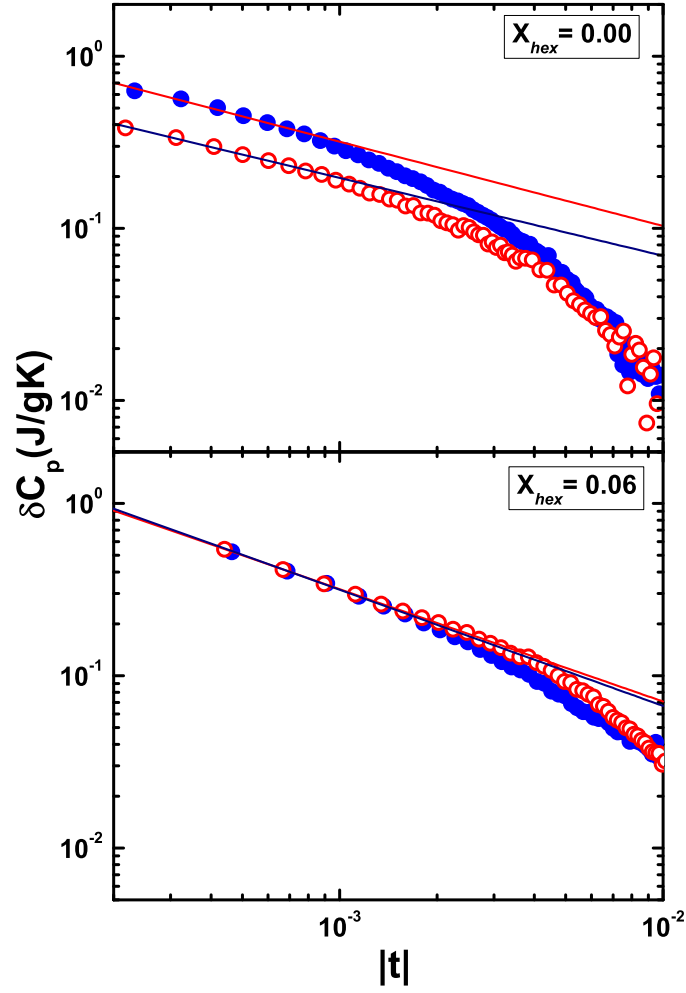


FIG. 6: Upper panel: Excess specific heats associated to N -SmA phase transition as a function of reduced temperature for pure 8CB for $T < T_c$ (\bullet) and for $T > T_c$ (\circ). Lower panel: Excess specific heats associated to N -SmA phase transition as a function of reduced temperature for hexane mole fraction $x_{hex} = 0.06$ for $T < T_c$ (\bullet) and for $T > T_c$ (\circ). Slope of the straight line in each graph gives the effective critical exponent α_{eff} .

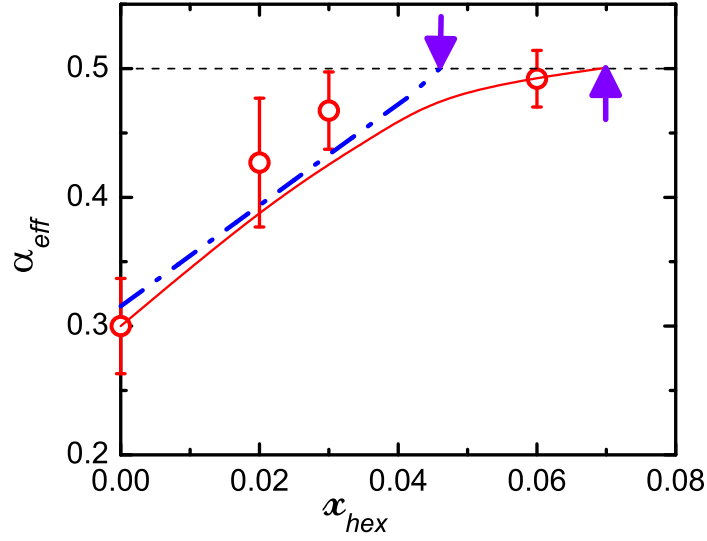


FIG. 7: The effective critical exponent as a function of hexane mole fraction. solid line represents the best estimate of α_{eff} as a function of x_{hex} . This line intersects the horizontal dashed line at the tricritical point, $x_{hex} \simeq 0.07$. The dashed-dot line is α_{eff} for 8CB+chex system from reference [19]. Vertical arrows indicate the location of the tricritical points for 8CB+chex (downward arrow) [19] and 8CB+hex(upward arrow).

Tables

TABLE I: Summary of the calorimetric results for pure and all 8CB+hex samples on heating. Shown are hexane molar fraction x_{hex} , N -SmA transition temperature T_{NA} , nematic range $\Delta T_N = T_{IN} - T_{NA}$ (in Kelvin), integrated enthalpy change δH_{NA}^* , imaginary enthalpy $\delta H_{NA}''$ (in J/g), McMillan's Ratio MR , and heat capacity maximum $h_M \cong \delta C_p^{max}(N - A)$ in $(JK^{-1}g^{-1})$.

x_{hex}	T_{NA}	ΔT_N	δH_{NA}^*	$\delta H_{NA}''$	MR	h_M
0.00	306.09 ± 0.06	7.11 ± 0.11	0.59 ± 0.06	—	0.977	0.78
0.02	304.42 ± 0.09	5.53 ± 0.59	0.99 ± 0.10	—	0.982	1.00
0.03	304.09 ± 0.08	5.03 ± 0.41	1.04 ± 0.10	—	0.984	1.45
0.06	304.21 ± 0.14	5.27 ± 0.50	0.73 ± 0.07	—	0.983	0.78
0.08	303.60 ± 0.16	4.46 ± 0.63	1.17 ± 0.12	0.28 ± 0.03	0.986	2.07
0.09	301.93 ± 0.17	3.23 ± 0.96	1.64 ± 0.16	0.29 ± 0.03	0.989	2.94
0.12	301.09 ± 0.08	2.53 ± 1.41	1.55 ± 0.15	0.40 ± 0.04	0.989	1.96